OXFORD

SOT | Society of Toxicology
www.toxsci.oxfordjournals.org

ToxSci 20 Years

TOXICOLOGICAL SCIENCES, 161(1), 2018, 171–185

doi: 10.1093/toxsci/kfx208
Advance Access Publication Date: October 9, 2017
Research Article

# A Genome-wide Screening of Target Genes Against Silver Nanoparticles in Fission Yeast

Ah-Reum Lee,*[,1] Sook-Jeong Lee,†[,1] Minho Lee,‡ Miyoung Nam,* Sol Lee,* Jian Choi,* Hye-Jin Lee,* Dong-Uk Kim,§[,2] and Kwang-Lae Hoe*[,2]

*Department of New Drug Discovery and Development, Chungnam National University, Daejeon 34134, Republic of Korea; †Department of Bioactive Material Science, Chonbuk National University, Jeonju 54896, Republic of Korea; ‡Catholic Precision Medicine Research Center, College of Medicine, The Catholic University of Korea, Seoul 06591, Republic of Korea; and §Department of Aging Research Center, KRIBB, Daejeon 34141, Republic of Korea

[1]These authors contributed equally to this work.
[2]To whom correspondence should be addressed at Department of Aging Research Center, KRIBB, Daejeon 34141, Republic of Korea, E-mail: Dongku@kribb.re.kr (Dong-Uk Kim) and Department of New Drug Discovery and Development, Chungnam National University, Daejeon 34134, Republic of Korea, E-mail: kwanghoe@cnu.ac.kr (Kwang-Lae Hoe)

## ABSTRACT

To identify target genes against silver nanoparticles (AgNPs), we screened a genome-wide gene deletion library of 4843 fission yeast heterozygous mutants covering 96% of all protein encoding genes. A total of 33 targets were identified by a microarray and subsequent individual confirmation. The target pattern of AgNPs was more similar to those of $AgNO_3$ and $H_2O_2$, followed by Cd and As. The toxic effect of AgNPs on fission yeast was attributed to the intracellular uptake of AgNPs, followed by the subsequent release of $Ag^+$, leading to the generation of reactive oxygen species (ROS). Next, we focused on the top 10 sensitive targets for further studies. As described previously, 7 nonessential targets were associated with detoxification of ROS, because their heterozygous mutants showed elevated ROS levels. Three novel essential targets were related to folate metabolism or cellular component organization, resulting in cell cycle arrest and no induction in the transcriptional level of antioxidant enzymes such as Sod1 and Gpx1 when 1 of the 2 copies was deleted. Intriguingly, *met*9 played a key role in combating AgNP-induced ROS generation via NADPH production and was also conserved in a human cell line.

**Key words:** fission yeast; *met*9; NADPH; ROS; silver nanoparticles; systematic screening.

Silver (Ag) metal and soluble silver compounds have been used for a variety of applications. Particularly, silver nanoparticles (AgNPs) have been widely used in industrial, household, and healthcare-related products due to their potent antimicrobial activity (Chen and Schluesener, 2008). However, the biocidal properties of AgNPs have the same potential to adversely affect many organisms including human beings and beneficial microorganisms in the environment. In an attempt to find genes related to AgNP-induced cytotoxicity, many experiments have been performed using a variety of human cell lines (Asharani *et al.*, 2012; AshaRani *et al.*, 2009), nematode (Roh *et al.*, 2009), and plants (Nair and Chung, 2014). AgNP-induced toxicity in bacteria through humans is via mitochondrial dysfunction, reactive oxygen species (ROS) release, and oxidative damage (AshaRani *et al.*, 2009). It has been well established that the most prominent mechanism of AgNP-induced cytotoxicity is via ROS induction, subsequently resulting in oxidative stress (Carlson *et al.*, 2008). Increased cellular levels of ROS cause oxidative stress, thereby

damaging DNA, lipids, and proteins (Halliwell and Aruoma, 1991; Jakobsson-Borin *et al.*, 1994; Stadtman, 1993). The more rapidly the area of nanoparticle-containing products grows in the market, the more studies addressing their toxicity mechanism with respect to human health and the environmental impact become urgently required.

To date, the toxic effects of AgNPs have been attributed to the intracellular release of $Ag^+$ from AgNPs (Damm and Münstedt, 2008; Gliga *et al.*, 2014). Notably, $Ag^+$ is well known to exhibit bactericidal effects via a mechanism similar to that by AgNPs (Drake and Hazelwood, 2005; Yamanaka *et al.*, 2005). $Ag^+$ interacts with the cell membrane, nucleic acids, and proteins and results in membrane damage and inhibition of the thiol-containing enzymes and proteins (Jung *et al.*, 2008).

Yeast species have long been model organisms for studying cell division and the cell cycle due to their facile genetics (Nurse, 1994). Particularly, the rod-shaped fission yeast *Schizosaccharomyces pombe* provides an excellent model system to study cell morphogenesis and cell division cycles. We have constructed a genome-wide gene deletion library in fission yeast after budding yeast *Saccharomyces cerevisiae* with built-in bar codes in a gene-specific manner (Kim *et al.*, 2010). The availability of bar codes in yeasts has opened the research area for parallel analysis, allowing researchers to find sensitive or resistant target genes against chemicals by the principle of drug-induced haploinsufficiency (Lum *et al.*, 2004). So far, most previous genome-wide screening for stress inducers has been applied with a haploid gene deletion library consisting of only nonessential genes (Guo *et al.*, 2016; Kennedy *et al.*, 2008). However, screening strategies using a heterozygous gene deletion library have proven to be more powerful, as they cover all the genes, including essential genes in addition to nonessential genes (Han *et al.*, 2013; Kim *et al.*, 2010; Lum *et al.*, 2004).

In this study, we systematically screened for target genes against AgNPs using our heterozygous gene deletion library in fission yeast. We suggest that the toxic effects of AgNPs are attributed to the intracellular release of silver ions, as reported previously. For the first time, we report that several novel essential genes are critical for tolerance to AgNP-induced cytotoxicity in addition to the previously reported nonessential genes. Intriguingly, this study is the first to show that the *met*9 essential gene is critical for the cellular defense against AgNP-mediated toxicity in fission yeast via the regulation of NADPH and that its relevance is conserved in a human cell line.

## MATERIALS AND METHODS

*Chemicals and cell culture*. AgNPs, AccuSilverSol silver nano colloid in water (Catalog no. TS-2010-1; stock solution = 1%; diameter = 17.4 nm), were purchased from Bioneer (Daejeon, Korea). AgNPs, $AgNO_3$, N-acetylcysteine (NAC), and 2′, 7′-dichlorodihydrofluorescein diacetate ($H_2$DCFDA) were purchased from Wako Pure Chemical Industries (Osaka, Japan) and Molecular Probes (Eugene, Oregon), respectively. All other reagents and chemicals were purchased from Sigma-Aldrich (St. Louis, Missouri), unless otherwise stated. Yeast cells were cultivated in complete YES medium (0.5% yeast extract, 3% glucose, and appropriate amino acid supplements) or Edinburgh minimal medium with appropriate supplements at 30 °C unless otherwise specified (Moreno *et al.*, 1991). Human embryonic kidney (HEK) 293 cells were obtained from the Korean Cell Line Bank (Seoul, Korea). The cells were maintained in Dulbecco's Modified Eagle's Medium supplemented with 10% fetal bovine serum and antibiotics (100 units/ml penicillin, 0.1 mg/ml streptomycin sulfate, 0.25 μg/ml amphotericin B) at 37°C in a humidified atmosphere containing 5% $CO_2$. All reagents and chemicals for cell culture were purchased from WELGENE (Gyeongsan, Korea) and Sigma-Aldrich, respectively, unless otherwise stated.

*Genome-wide screening of the heterozygous gene deletion library in fission yeast by microarray*. For the systematic screening of sensitive target genes for AgNPs, we used the heterozygous gene deletion library constructed in a previous study (Kim *et al.*, 2010). Briefly, the library was constructed by homologous replacement of each gene into the KanMX marker gene as a selection marker based on the parental strain of the SP286 wild-type (*ade6-M210/ade6-M216, leu1-32/leu1-32, ura4-D18/ura4-D18 h*$^+$*/h*$^+$). The library was pooled and aliquoted into 100 μl vials for each screen, and the vials were kept frozen at −80 °C until use. Notably, each deletion mutant has a pair (up- and down-tag) of unique built-in molecular bar codes for a parallel analysis. The systematic screening of AgNP target genes was performed as previously reported (Han *et al.*, 2013). Briefly, a vial of frozen pool was activated in 50 ml of YES media for 24–30 h up to $OD_{600} = 2$ (approximately $4.4 \times 10^7$ cells/ml). The cells were then diluted in 50 ml of YES media to $OD_{600} = 0.05$ and cultivated up to $OD_{600} = 1.6$ (approximately $3.5 \times 10^7$ cells) with or without AgNPs (0.2 μg/ml), which was repeated 4 times every 5 generations up to 20 generations. An aliquot of $3.5 \times 10^7$ cells was harvested every 5 generations and genomic DNA was prepared using the ZR-Fungal/Bacterial DNA kit (Zymo Research, Irvine, California). The microarray experiment was performed using a custom-made GeneChip (48 K KRIBB_SP2, ThermoFisherScientific, Waltham, Massachusetts) and the fluorescence-labeled probe prepared by PCR of the pair of bar codes (Kim *et al.*, 2010). Three independent microarray experiments were performed. The primary 44 target strains were selected by the criterion that the results indicated relative growth fitness (RF) < 0.9 ($p < .05$) twice.

*Confirmation of the primary target genes by spotting assay*. The primary candidates were confirmed one by one based on an individual growth analysis using a spotting assay. For the spotting assay, cells in log phase were diluted to $OD_{600} = 0.5$ in YES media and spotted in 5-fold serial dilutions onto YES agar plates with or without 0.2 μg/ml AgNPs. Their sensitivity against AgNPs was scored by the following criterion: severe (SSS) when their survival rate was decreased by more than 3 serial dilutions (>75-fold sensitivity); moderate (SS) by 2 to 3 serial dilutions (25- to 75-fold sensitivity); and mild (S) by 2 serial dilutions (<25-fold sensitivity). The total of 33 target genes was confirmed and subject to gene ontology (GO) analysis using GO term finder (http://go.princeton.edu/cgi-bin/GOTermFinder).

*Observation of cellular AgNPs*. The cellular uptake of AgNPs by yeast cells was measured using inductively coupled plasma mass spectrometry (ICP-MS) and visualized using transmission electron microscopy (TEM). Cells in the log phase were treated with AgNPs or $AgNO_3$ at the indicated concentrations for 12 h. The treated cells were washed 3 times with PBS (pH 7.4), harvested, and subjected to ICP-MS and TEM analyses. In order to quantify intracellular Ag that was absorbed by the cells, the harvested cells were digested by acid treatment using the HotBlock digestion system (Environmental Express, Charleston, South California). Briefly, $HNO_3$ was added to the sample, followed by irradiation at 110 °C for 5–6 h. After digestion, the samples were diluted with water and quantified using the ELAN DRC II ICPMS (PerkinElmer, Waltham, Massachusetts). The AgNPs accumulated inside the cells were also observed by TEM. Briefly, the harvested

cells were fixed in 2.5% glutaraldehyde in 0.1 M PBS (pH 7.4), followed by fixing in 2% osmium tetroxide in the same buffer for 1 h. The cells were dehydrated using a series of ethanol concentrations and subsequently embedded in the Epon 812 resin (Hexion, Columbus, Ohio). After sectioning the samples using an ultramicrotome (Leica Microsystems, Vienna, Austria), they were stained with uranyl acetate and lead citrate. The stained samples of AgNPs were placed onto a carbon-coated copper grid and air dried. The images were observed using the FEI Tecnai G2 T-20S TEM (FEI Europe B.V., Eindhoven, the Netherlands), equipped with the Gatan ORIUS SC1000 CCD camera.

*Cross-sensitivity comparison by hierarchical clustering*. For cross-sensitivity comparison, in addition to the top 10 target genes showing higher sensitivity than SS, 17 additional genes which were related to the relevant GO terms were used. The genes used were as follows: signal transduction (*win*1, *sty*1, *pap*1, *atf*1, and *wis*1 in addition to *wis*4, *mcs*4, and SPCC1827.07c), sulfur compound metabolism (*sua*1, *sir*1, *cys*12, *met*10, *cys*11, and *met*14 in addition to *hmt*2, *rdl*2, *gcs*1, and *gcs*2), (*met*11, *shm*2, *thf*1, *dfr*1, *mtd*1, and *fol*1 in addition to *met*9), and cellular component organization (*sfh*1 and *peg*1). Additionally, 35 genes were randomly selected and included in the above analysis. Their growth rate was measured by plating serial 5-fold dilutions onto YES plates supplemented with 0.2 μg/ml AgNPs, 0.4 μg/ml $AgNO_3$, 2 mM $H_2O_2$, 0.4 mM Cd, or 0.5 mM As. All experiments were performed at least 3 times. The results were analyzed by hierarchical clustering using Euclidean distance as the measure of similarity. R version 3.3.3 and R package "gplots" were used for analysis and visualization, respectively.

*Measurement of ROS levels and relative growth*. To measure intracellular ROS levels, the redox-sensitive green fluorescent $H_2$DCFDA probe was used along with propidium iodide (PI) dye to distinguish living cells from dead ones. Briefly, cells were exposed to AgNPs for 3 h at 30 °C and washed twice with PBS (137 mM NaCl, 10 mM phosphate, 2.7 mM KCl, pH 7.4). The cells were then incubated with 40 μM $H_2$DCFDA for 1 h and 3 μg/ml PI for 10 min at 30 °C in the dark. fluorescence-activated cell sorting (FACS) analysis was utilized to detect the ROS probe using a FACSCANTO II (BD Biosciences, Franklin Lakes, New Jersey) with excitation or emission wavelengths of 488 or 525–550 nm, respectively. A total of 10 000 PI-negative cells were used for each analysis and PI-stained, dead cells were excluded from analysis. To measure the relative growth rate in liquid media, yeast strains were activated overnight at 30 °C to saturation using a DeepWellMaximizer bioshaker (TAITEC, Saitama-ken, Japan). The cells were then diluted to $OD_{600} = 0.05$ with YES media in 96-deep-well plates with or without 0.2 μg/ml AgNPs, cultivated again, and growth rate was measured by determining the $OD_{600}$ using an Epoch microplate spectrophotometer (BioTek, Winooski, Vermont).

*Observation of cell morphology and analysis of cell cycle*. Phenotypic changes of cells in the presence of 0.2 μg/ml AgNPs were observed by a fluorescent microscope (Leica DM5000B; Wetzlar, Germany) equipped with a digital CCD camera (DFC350FX). Cell nuclei and septa were visualized by staining using 1 μg/ml 4′, 6-diamidino-2-phenylindole (DAPI) and 50 μg/ml Calcofluor-white, respectively. For cell cycle analysis by FACS, cells were synchronized in G1/S phase by treatment with 11 mM hydroxyurea (HU) for 4 h and were allowed to restart the cell cycle in the presence of 0.2 μg/ml AgNPs upon release from HU. After incubation for the indicated time, the cells were harvested and then stained with 4 μg/ml PI after a 70% ethanol fixation (Moreno *et al.*, 1991). FACS analysis was performed using the FACSCANTO II with $1 \times 10^4$ cells. The results were analyzed using BD FACSDiva software (BD Biosciences) by employing regions with FL2 area versus FL2 width.

*Measurement of transcriptional level*. To measure the transcriptional level of antioxidant enzymes, quantitative PCR (q-PCR) was performed. Briefly, mRNA was extracted with TRIzol (ThermoFisherScientific) and cDNA was synthesized from the extracted mRNA using the Quantiscript reverse transcriptase (Qiagen, Hilden, Germany) according to the manufacturer's instruction. Approximately 100 ng cDNA was amplified by PCR using iQ SYBR Green Supermix in the CFX96 Touch Real-Time Detection System (Bio-Rad, Hercules, California). The PCR primers were synthesized by Bioneer. The primer sequences of fission yeast genes were as follows: *sod*1, forward 5′-GTCACTCGC TTCCTAGTACAAAG-3′ and reverse 5′-CCCATAATGAACAAACC TCTCAGTAT-3′; *gpx*1, forward 5′-AGCGAGCAAATGTGGATTC A-3′ and reverse 5′-AATTGAGCGATTTCTTCGTCAGA-3′; *act*1 (a normalization control), forward 5′-TCCAACCGTGAGAAGATGAC T-3′ and reverse 5′-CGACCAGAGGCATACAAAGAC-3′. The primer sequences of human genes are as follows: *MTHFR*, forward 5′-TGGAAGACACATTGGAGC-3′ and reverse 5′-CAAGAGAA GCAGCACTGT-3′; β-actin as a normalization control, forward 5′-ATCGTCCACCGCAAATGCTTCTA-3′ and reverse 5′-AAGCCA TGCCAATCTCATCTTGTT-3′.

*Measurement of NADP and/or NADPH concentration*. To measure NADP/NADPH concentration, the NADP/NADPH quantification colorimetric kit was used by following the manufacturer's protocol (catalog no. K347-100; BioVision Inc; Milpitas, California). To measure both NADP and NADPH, $4 \times 10^6$ cells were harvested and lysed in extraction buffer. An NADP cycling mix was added and incubated to convert NADP to NADPH. Finally, NADPH developer was added, and the $OD_{450}$ was measured after a reaction for 1–4 h. NADPH concentration was calculated using a standard curve of NADPH. To measure NADPH only, NADP was decomposed from the cell extracts by heating samples to 60 °C for 30 min. Samples were normalized using the BCA protein assay kit (ThermoFisherScientific).

*siRNA assay*. To mimic the heterozygous effect of yeast in humans, gene transcription was reduced by siRNA knockdown. The siRNA oligonucleotides of *MTHFR* and a negative control (scrambled, catalog no. 4390843) were purchased from ThermoFisherScientific. Sequences of *MTHFR* were as follows: sense 5′-GCACAUCCGAAGUGAGUUU (dTdT)-3′ and antisense 5′-AAACUCACUUCGGAUGUGC (dTdT)-3′. The oligonucleotides were transfected into cells using the HiPerFect kit (Qiagen) according to the manufacturer's instruct. After incubation for 72 h, the extent of knockdown by siRNA was measured by q-PCR.

*MTT assay and 8-OHdG measurement*. HEK293 cells ($2 \times 10^4$ cells/well in a 48-well plate) were treated with 0.6 μg/ml AgNPs, and then their viability was measured using an MTT-based cell viability assay. To measure oxidative DNA damage, 8-hydroxy-2′-deoxyguanosine (8-OHdG) was analyzed using the OxiSelect Oxidative DNA damage ELISA kit (Cell Biolabs Inc, San Diego, California) by following the manufacturer's protocol. Briefly, genomic DNA was converted to single-stranded DNA and 8-OHdG was quantified using a standard curve by quantitative ELISA assay.

**Table 1.** List of the 33 AgNP Targets Screened

| GO (Biological Process)[a] Gene Name/Systematic ID | Gene Description[b] | Sensitivity[c] | | E/V[d] |
|---|---|---|---|---|
| | | AgNPs | $AgNO_3$ | |
| **Sulfur compound metabolism ($p < 8.71E-04$)** | | | | |
| *gcs*1 | Glutamate-cysteine ligase | SSS | SS | V |
| *gcs*2 | Glutamate-cysteine ligase regulatory subunit | SS | SS | V |
| *pcs*2 | Phytochelatin synthetase | S | S | V |
| *hmt*2 | Sulfide-quinone oxidoreductase | SS | S | V |
| *rdl*2 | Mitochondrial thiosulfate sulfurtransferase | SS | S | V |
| *srx*1 | Sulfiredoxin | S | S | V |
| **Signal transduction ($p < 1.12E-04$)** | | | | |
| *mcs*4 | Signal transduction response regulator | SS | S | V |
| *wis*4 | MAP kinase kinase kinase | SS | SS | V |
| SPCC1827.07c | SPX/EXS domain protein | SS | S | V |
| **One-carbon metabolism by folate** | | | | |
| *met*9 | Methylenetetrahydrofolate reductase | SSS | SSS | E |
| **Cellular component organization** | | | | |
| *peg*1 | CLASP family microtubule-associated protein | SSS | S | E |
| *sfh*1 | RSC complex subunit | SS | S | E |
| *stg*1 | SM22/transgelin-like actin modulating protein | S | S | V |
| **Gene expression** | | | | |
| *clr*4 | Histone H3 lysine methyltransferase | S | S | V |
| *sup*45 | Translation release factor eRF1 | S | S | E |
| *tif*223 | eIF2B gamma subunit | S | NS | E |
| *rpl*31 | 60S ribosomal protein L31 | S | S | E |
| *sks*2 | HSP, ribosome associated Molecular chaperone | S | S | V |
| *lsg*1 | Lsk1 complex gamma subunit | S | S | V |
| SPAC4G8.09 | Mitochondrial leucine-tRNA ligase | S | S | E |
| **Transport** | | | | |
| *trk*1 | $K^+$ transmembrane transporter | S | S | V |
| *msn*5 | Karyopherin | S | NS | V |
| *vps*1 | Dynamin family protein | S | S | V |
| SPBC887.12 | P-type ATPase | S | S | E |
| **Unclassified** | | | | |
| *ebs*1 | EST1 family NMD pathway protein | S | S | V |
| *spo*9 | Farnesyl pyrophosphate synthetase | S | S | V |
| *gid*2 | GID complex ubiquitin-protein ligase E3 subunit | S | NS | V |
| *adn*1 | Adhesion defective protein | S | S | V |
| *psr*1 | NLI interacting factor family phosphatase | S | NS | V |
| SPCC63.13 | DNAJ domain protein | S | S | V |
| SPAC1805.14 | Schizosaccharomyces specific protein | S | S | V |
| SPBC1604.12 | Schizosaccharomyces specific phosphoprotein | S | S | V |
| SPAC9.02c | Polyamine N-acetyltransferase | S | S | V |

[a]GO analysis in terms of the biological process has been analyzed using GO term finder (http://go.princeton.edu/cgi-bin/GOTermFinder).
[b]Gene description is same as indicated in fission yeast PomBase (http://www.pombase.org) and UniProt (http://www.uniprot.org).
[c]Sensitivity are classified as follows: severe (SSS), moderate (SS), mild (S), and not sensitive (NS).
[d]Dispensability data are from the *Schizosaccharomyces pombe* PomBase (http://www.pombase.org) and confirmed by tetrad analysis in this study. 'V' and 'E' represent nonessential and essential genes, respectively.

*Statistical analysis*. All experiments were performed using triplicate samples and repeated at least 3 times. Data are presented as mean ± SD, and statistical comparisons between groups were performed using a Student's *t*-test. For multiple comparisons among groups, 2-way ANOVA with the Student-Newman-Keuls method was performed using GraphPad Prism (La Jolla, California). The *p*-values $< .05$ were considered significant.

## RESULTS

### *Primary Genome-Wide Target Screening and Secondary Individual Confirmation Revealed 33 AgNP Target Genes*

Through the primary genome-wide screening against AgNPs, 44 target strains were selected with RF $< 0.9$ ($p < .05$) compared with the wild-type control in Table 1. Finally, 33 target genes were confirmed by the spotting assay as shown in Table 1. They consisted of 3 severe (SSS), 7 moderate (SS), and 23 mild (S) targets as measured by sensitivity, and 25 non-essential and 8 essential targets as measured by gene dispensability. Additionally, we observed 20 strains resistant to AgNPs (RF $> 1.1$, $p < .05$) as shown in Supplementary Table 1. Most AgNP-resistant target genes were related to the following processes: gene expression, cellular component organization, localization, and lipid metabolic process.

According to the GO analysis for biological process, the 33 target genes were related to the following processes: sulfur compound metabolism (*gcs*1, *gcs*2, *hmt*2, *rdl*2, *pcs*2, and *srx*1; $p < 8.71E-4$), signal transduction (*mcs*4, *wis*4, and SPCC1827.07c;

**Table 2.** List of the Top 10 AgNP Targets

| GO[a] (Biological Process) | Gene name/Systematic ID (Human Ortholog[b]) | Sensitivity[c] (E/V) | Cross-sensitivity | | |
|---|---|---|---|---|---|
| | | | Stress[d] | Organism | Ref[e] |
| **Sulfur compound metabolism** | | | | | |
| Glutathione biosynthetic process | *gcs*1 (GCLC) | SSS (V) | Cd | Fission yeast | Kennedy *et al.* |
| | | | $H_2O_2$, Cd | Fission yeast | Pluskal *et al.* |
| | | | AgNPs | Human | Kang *et al.* |
| | *gcs*2 (GCLM) | SS (V) | Cd | Fission yeast | Kennedy *et al.* |
| | | | AgNPs | Human | Kang *et al.* |
| Cellular sulfide ion homeostasis | *hmt*2 (SQRDL) | SS (V) | Cd | Fission yeast | Kennedy *et al.* |
| | | | Cd, As | Fission yeast | Guo *et al.* |
| | | | $H_2O_2$, Cd | Fission yeast | Pluskal *et al.* |
| | | | $H_2S$ | Human | Hourihan *et al.* |
| | *rdl*2 (TSTD1) | SS (V) | $Na_2Se$ | Budding yeast | Peyroche *et al.* |
| | | | $H_2S$ | Human | Melideo *et al.* |
| **Signal transduction** | | | | | |
| Stress-activated MAPK cascade | *mcs*4 | SS (V) | Cd | Fission yeast | Kennedy *et al.* |
| | | | As | Fission yeast | R-G *et al.* |
| | *wis*4 (MAP3K4) | SS (V) | Cd | Fission yeast | Kennedy *et al.* |
| | | | $H_2O_2$ | Fission yeast | R-G *et al.* |
| Signaling | SPCC1827.07c (XPR1) | SS (V) | Metals | Budding yeast | Yu *et al.* |
| | | | Mn | Budding yeast | Chesi *et al.* |
| **One-carbon metabolism by folate** | | | | | |
| Tetrahydrofolate interconversion | *met*9 (MTHFR) | SSS (E) | Vn | Human | Visalli *et al.* |
| | | | AgNPs | Fission yeast | This study |
| **Cellular component organization** | | | | | |
| Chromatin organization | *sfh*1 | SS (E) | AgNPs | Fission yeast | This study |
| Cytoskeleton organization | *peg*1 | SSS (E) | AgNPs | Fission yeast | This study |

[a]GO analysis in terms of the biological process has been analyzed using GO term finder (http://go.princeton.edu/cgi-bin/GOTermFinder).
[b]Data of human orthologs are from the HomoloGene or Ensembl database (https://www.ncbi.nlm.nih.gov/homologene or http://www.ensembl.org).
[c]Sensitivity are classified as follows: severe (SSS), moderate (SS), and mild (S).
[d]Abbreviation of stresses used in the study are as follows: AgNPs (silver nanoparticles), As (Arsenite), Cd (Cadmium), and Vn (Vanadium).
[e]References represent the previous reports saying that the genes are associated with metal resistance and/or response to oxidative stress in yeasts and/or human.

$p < 1.12E\text{-}4$), one-carbon metabolism by folate (*met*9), cellular component organization (*peg*1, *sfh*1, and *stg*1), gene expression (*clr*4, *sup*45, *tif*223, *rpl*31, *sks*2, *lsg*1, and SPAC4G8.09), transport (*trk*1, *msn*5, *vps*1, and SPBC887.12), and unclassified process (*ebs*1, *spo*9, *gid*2, *adn*1, *psr*1, SPCC63.13, SPAC1805.14, SPBC1604.12, and SPAC9.02c). Among the GO terms described, the "sulfur compound metabolism" and "signal transduction" were significantly enriched, suggesting that the pathways related to reducing power production and stress signaling were important for AgNP tolerance. In accordance, other previous reports have described that both stress-activated mitogen-activated protein kinase (MAPK) cascade and redox homeostasis, including biosynthesis of glutathione and other reducing power agents are critical for the detoxification of AgNPs (Rodriguez-Gabriel and Russell, 2005). In particular, the sulfur compound metabolism and one-carbon metabolism by folate were previously reported to be involved in the production of reducing powers such as GSH (Guo *et al.*, 2016) and NADPH (Fan *et al.*, 2014).

For further studies, out of the 33 targets, we narrowed down the number of AgNP targets to 10 under the criterion of sensitivity higher than moderate (ie, SS or SSS), consisting of 7 nonessential and 3 essential genes. According to GO analysis of the 10 targets for the biological process, the 7 nonessential genes fall under sulfur compound metabolism (*gcs*1, *gcs*2, *hmt*2, and *rdl*2) or stress-activated MAPK kinase cascade/signaling (*mcs*4, *wis*4, and SPCC1827.07c), and the 3 essential genes fall under one-carbon metabolism by folate (*met*9) or (*sfh*1 and *peg*1) (Table 2). In accordance with the results, all 7 nonessential genes have been previously reported to be related to metal resistance and/or response to oxidative stress (see references in Table 2). Especially, our previous study also indicated that *hmt*2 plays a key role for Cd tolerance by the elimination of ROS via CoQ10 in the plasma membrane (Kennedy *et al.*, 2008). However, the 3 essential genes have not been previously described as AgNP targets. Additionally, we analyzed whether the 33 AgNP targets were also sensitive to $Ag^+$ (Table 1). The targets for AgNPs and $Ag^+$ were observed to be the same except 4 target genes. These results suggest that the cytotoxic effect of AgNPs may be potentially attributed to $Ag^+$ released from AgNPs.

### *AgNPs Penetrate Yeast Cells and Release $Ag^+$*

The above results prompted us to analyze whether AgNPs could penetrate cells and subsequently cause cytotoxicity. TEM images showed AgNPs inside the cells, suggesting that AgNPs could penetrate the yeast cells (Figure 1A). AgNPs were also observed in cellular organelles, such as nucleus and vesicle-like structures, but not at the cell wall. Next, the amount of intracellular Ag and its associated cytotoxicity were compared between the AgNP- and $AgNO_3$-treated cells (Figure 1B). The amount of Ag in the AgNP-treated cells was approximately 2-fold higher than that in the $AgNO_3$-treated cells, and it accumulated in a concentration-dependent manner. Based on these results, we concluded that the cytotoxicity of AgNPs was higher than that of $AgNO_3$ at the indicated concentrations (Figure 1C). These

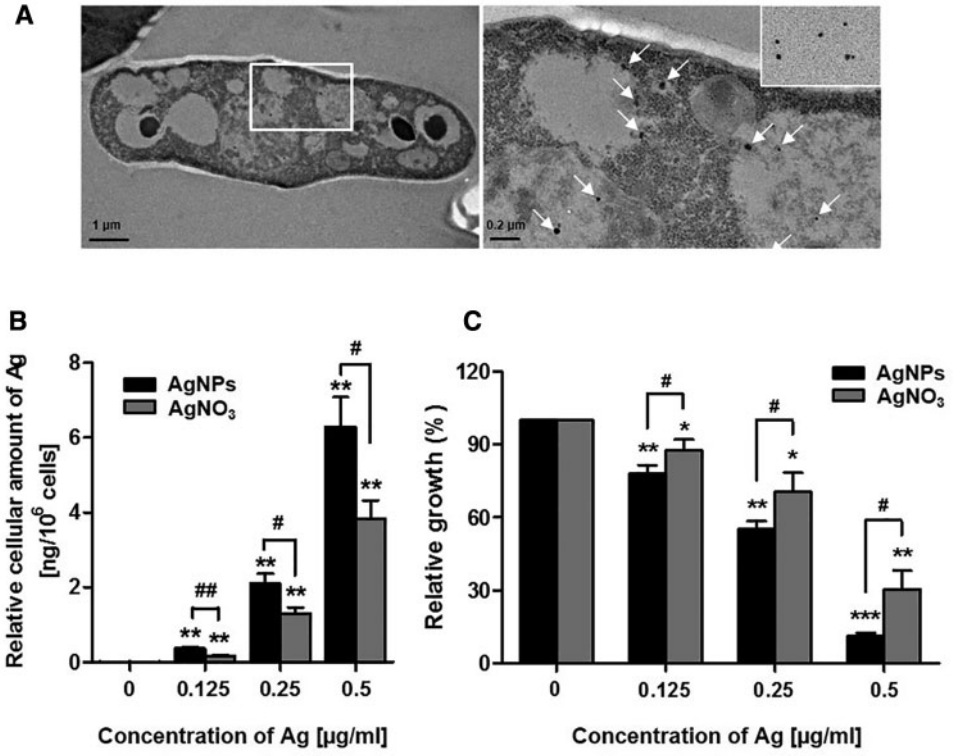


**Figure 1. Cellular uptake of silver nanoparticles (AgNPs) and $Ag^+$ by yeast cells.** A, Observation of AgNPs in yeast cells by transmission electron microscopy (TEM). A representative picture showing AgNPs inside the cells (left). AgNPs were observed inside the cells (white arrows), upon magnification of the area enclosed within the white inset (right). Yeast cells were treated with 0.25 μg/ml AgNPs for 12 h and observed by TEM. B, Cellular uptake of AgNPs or $AgNO_3$ in fission yeast. Cellular amounts of total Ag were measured by inductively coupled plasma mass spectrometry ($n = 3$; $**p < .01$, AgNP- or $AgNO_3$-treated vs untreated control cells; $\#p < .05$ and $\#\#p < .01$, AgNP-treated vs $AgNO_3$-treated cells). C, Cytotoxic effects of AgNPs and $AgNO_3$. The cells were treated at the indicated concentrations of AgNPs or $AgNO_3$ for 12 h, and their relative growth was analyzed by measuring $OD_{600}$ ($n = 3$; $*p < .05$, $**p < .01$, and $***p < .001$, AgNP- or $AgNO_3$-treated vs untreated control cells; $\#p < .05$, AgNP- vs $AgNO_3$-treated cells).

results also suggest that the cytotoxic effect of AgNPs is attributed to $Ag^+$ released from these NPs.

### *Target Pattern of AgNPs Is More Similar to Those of $AgNO_3$ and $H_2O_2$*

To elucidate the mechanism of action of the AgNP targets, we determined which stress is most similar to AgNPs (Figure 2). To increase the resolution power of cross-sensitivity, the 17 potential target genes associated with relevant GO terms and 35 randomly selected genes, in addition to the 10 target genes, were included. As shown by the hierarchical clustering analysis, the target pattern of AgNPs was more similar to those of $AgNO_3$ and $H_2O_2$ than to those of the metals (Cd or As). However, evidence suggests that the metal stimulants also elicit oxidative stress for inducing cellular toxicity (Valko *et al.*, 2005) (Table 2). The GO terms of target genes were related to biological processes such as stress-activated signaling and stress defense metabolism. Intriguingly, only 3 targets were observed to be sensitive to AgNPs among the 35 randomly selected targets, suggesting that the primary target screening using microarray was useful, despite not accounting for the missing targets. Taken together, AgNP-induced cytotoxicity is potentially attributed to ROS, as reported previously.

### *AgNP-Induced Growth Inhibition Is Attributed to an Increased Cellular Level of ROS*

The above results prompted us to evaluate the relationship between AgNP-induced cytotoxicity and their cellular ROS level. Upon measuring the relative cellular level of ROS induced by AgNPs, all the top 10 target strains produced higher levels of ROS ($p < .001$) compared with the wild-type control (Figure 3A). At the same time, treatment with AgNPs also significantly inhibited the relative growth of these strains (Figure 3B). Furthermore, pretreatment with the antioxidant NAC completely abrogated the AgNP-induced growth inhibition as described previously (Bell and Kramer, 1999; Navarro *et al.*, 2008; Zhang *et al.*, 2011). Taken together, the AgNP-induced cytotoxicity is attributed to ROS generation.

### *Three Essential AgNP Target Genes Are Related to Cell Cycle Progression via ROS*

In this study, for the first time the 3 essential target genes, *met*9, *sfh*1, and *peg*1, have been reported to be related to AgNP-induced cytotoxicity. Therefore, the effects of AgNP treatment on cell morphology and cell cycle were observed by microscopy (Figure 4A) and FACS analysis (Figure 4B). Microscopic analysis showed that cell shape was elongated with irregular thick septa, which is a morphological hallmark of G2/M cell cycle arrest. When observed by FACS after HU release, the cell cycle showed a delayed time lag in the transition from 4 °C to 8 °C (the arrows in Figure 4B) owing to a G2/M cell cycle arrest (Kang *et al.*, 2012). As shown in the lower panels of Figures 4A and 4B, the effect of AgNPs on cell morphology and cell cycle was abrogated by NAC pretreatment. The results suggest that ROS induced by AgNPs caused the observed effects on cell morphology and cell cycle.

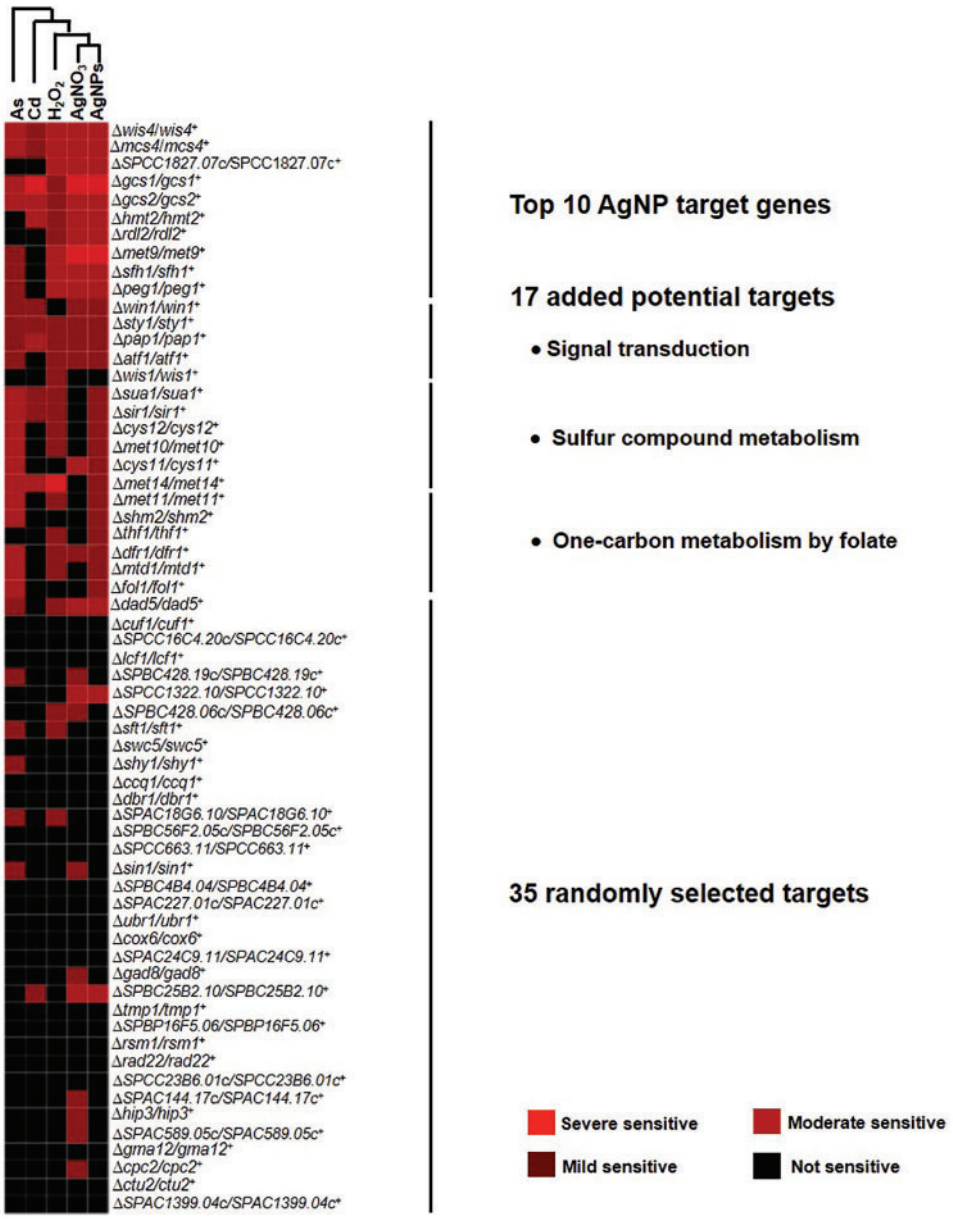


**Figure 2. Cross-sensitivity comparison of AgNP targets with those of the other stress inducers**. Using hierarchical clustering analysis, the target pattern of AgNPs was compared with those of the other stress inducers, such as AgNPs, $AgNO_3$, $H_2O_2$, Cd, and As. For this analysis, 62 heterozygous deletion strains including those for 10 AgNP targets, 17 potentially related targets associated with similar GO terms as those of the 10 AgNP targets (see "Materials and Methods"), and 35 randomly selected targets were used. A list of the 35 randomly selected targets has been shown in this figure.

### *The* met9 *Gene Is Related to NADPH Production*

There is an accumulating body of evidence that oxidative stress affects the transcriptional level of many antioxidant defense enzymes in fission yeast (Chung *et al.*, 2004; Lee *et al.*, 2002). In this regard, the intracellular level of reducing power molecules such as GSH regulates the transcriptional level of antioxidant enzymes (Farrugia and Balzan, 2012; Grant, 2001). Therefore, we examined the effects of AgNPs in the transcriptional induction of the first-line antioxidant enzymes such as *sod*1 and *gpx*1. As shown in Figure 5A, all 3 heterozygous deletion strains (*met*9, *sfh*1, and *peg*1) showed a similar transcriptional pattern of *sod*1 and *gpx*1. Compared with the wild-type control, the 3 common essential targets showed no discrete transcriptional induction of *sod*1 and *gpx*1 at 4 h after AgNP treatment. This may be because all the 3 heterozygotes with a single copy of the respective essential gene showed ROS induction resulting in chromatin/cytoskeleton stress (Perrone *et al.*, 2008; Uffenbeck and Krebs, 2006) or reducing power shortage (Fan *et al.*, 2014) resulting in the lack of transcriptional induction of the antioxidant enzymes against in response to AgNP treatment.

As all enzymatic or nonenzymatic antioxidants basically require NADPH as a reducing power (Birben *et al.*, 2012), the above results prompted us to check the cellular level of NADPH in the 3 heterozygous strains in response to AgNP treatment (Figure 5B). Normally, AgNP treatment of the control strain increased the $NADP^+$/NADPH ratio by 2-fold as the oxidative condition consumed NADPH for the supply of antioxidant enzymes. Similarly, after AgNP treatment, the heterozygote with a single copy of the essential gene *sfh*1 or *peg*1 displayed a 2- to 4-fold increase in the $NADP^+$/NADPH ratio. Intriguingly, AgNP treatment

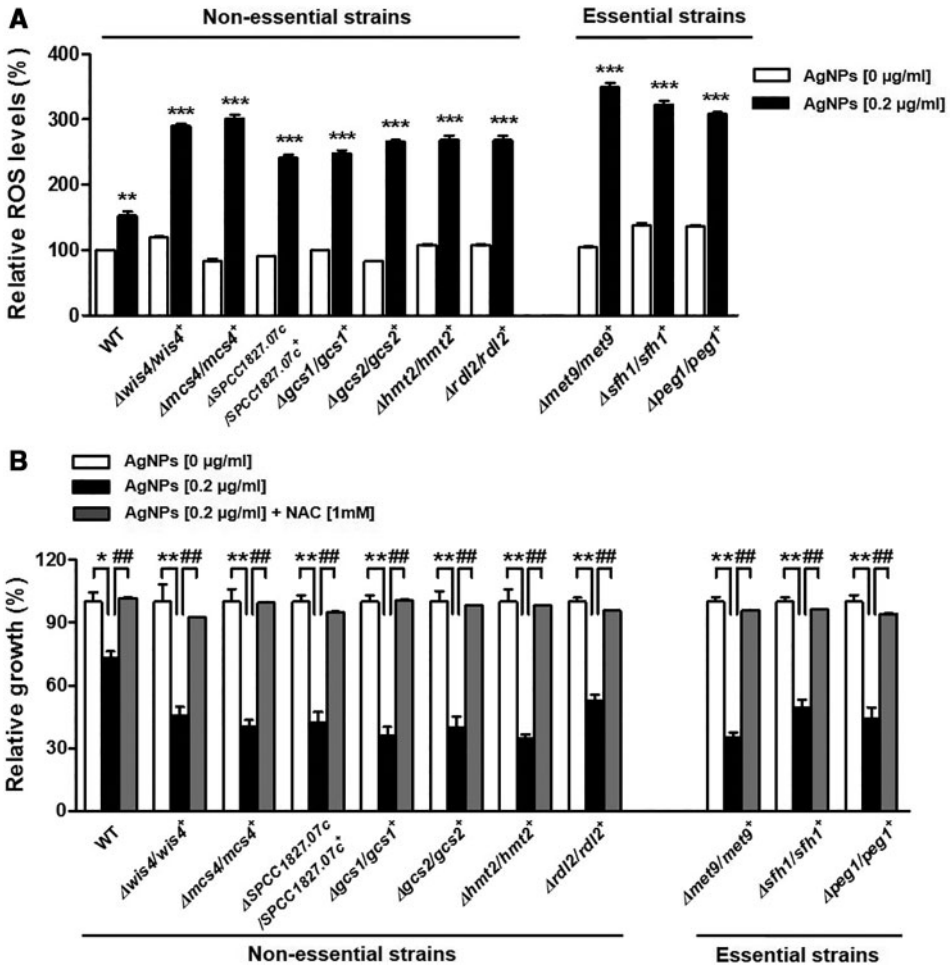


**Figure 3. AgNP-induced growth inhibition via reactive oxygen species (ROS) in the top 10 AgNP targets**. A, Quantitative analysis of ROS induced by AgNPs in the top 10 AgNP target heterozygotes. Cells were treated with 0.2 μg/ml of AgNPs for 3 h, and the amount of ROS induced by AgNPs was analyzed by flow cytometry using untreated wild-type cells as a control ($n = 3$; $^{**}p < .01$ and $^{***}p < 0.001$ treated vs untreated control cells). B, Quantitative analysis of growth inhibition by AgNPs in the top 10 AgNP target heterozygotes. Cells were treated with 0.2 μg/ml of AgNPs for 9 h, and their relative growth was analyzed by measuring the $OD_{600}$ using a microplate reader ($n = 3$; $^{*}p < .05$ and $^{**}p < .01$, AgNP-treated vs untreated control). Next, cells were pretreated with 1 mM N-acetylcysteine (NAC) prior to AgNP treatment and its effects were compared ($n = 3$; $^{\#\#}p < .01$, NAC-pretreated vs not pretreated cells).

of a heterozygote with a single copy of the essential *met*9 gene resulted in a shortage of NADPH reducing power, as judged by a 28-fold increase in the $NADP^+$/NADPH ratio which is 7 times greater induction than was observed for a heterozygote with a single copy of the essential *sfh*1 or *peg*1 gene. The results suggest that *met*9 plays a key role for NADPH production in the defense against oxidative stress by AgNPs. In accordance with the results, a recent paper has reported that almost half of NADPH production is related to a folate pathway containing the MTHFR (methylenetetrahydrofolate reductase, human ortholog of *met*9) gene in human cell lines (Fan *et al.*, 2014).

### *Role of* met9 *Is Conserved in a Human Cell Line*

We next determined whether the role of the 3 essential genes as AgNP targets was conserved in humans. According to the NCBI HomoloGene database, *MTHFR* gene, which sits at a gateway for both methionine and folate cycles, was revealed as the human ortholog of the fission yeast *met*9 gene, which is closely associated with both NADPH production and amino acid/DNA synthesis (Fodinger *et al.*, 2000). Unfortunately, we could not find the human ortholog of *sfh*1 or *peg*1. Therefore, we focused on the functional conservation of fission yeast *met*9 in humans.

To mimic the heterozygous effect of fission yeast in humans, we employed siRNA knockdown in HEK293 cells. As shown in Figure 6A, the transcriptional level of the *MTHFR* knockdown cells showed 34% expression of the control (scrambled), as judged by a quantitative real-time PCR (qRT-PCR) using β-actin as a normalization control. At first, we checked whether knockdown of *MTHFR* induced ROS in response to AgNP treatment (Figure 6B). As expected, the AgNP treatment of the *MTHFR* knockdown cells showed a significant increase in the ROS induction by 30% compared with the scrambled cells. Furthermore, the phenomenon was completely abrogated by NAC pretreatment. Next, we further evaluated the effects of AgNP-induced ROS on DNA damage (Figure 6C), cell survival rate (Figure 6D), and cell cycle (Figure 6E). Upon measuring the level of 8-OHdG adducts (Figure 6C) as an established marker of oxidative stress-induced DNA lesions (Cadet *et al.*, 2003), the AgNP treatment in the *MTHFR* knockdown cells resulted in a significant increase in the level of 8-OHdG adducts by 30% compared with the levels observed in scrambled cells. In accordance with the increased DNA damage, the AgNP treatment of the *MTHFR* knockdown cells showed a significant 40% decrease in cell viability compared with the viability of scrambled cells,

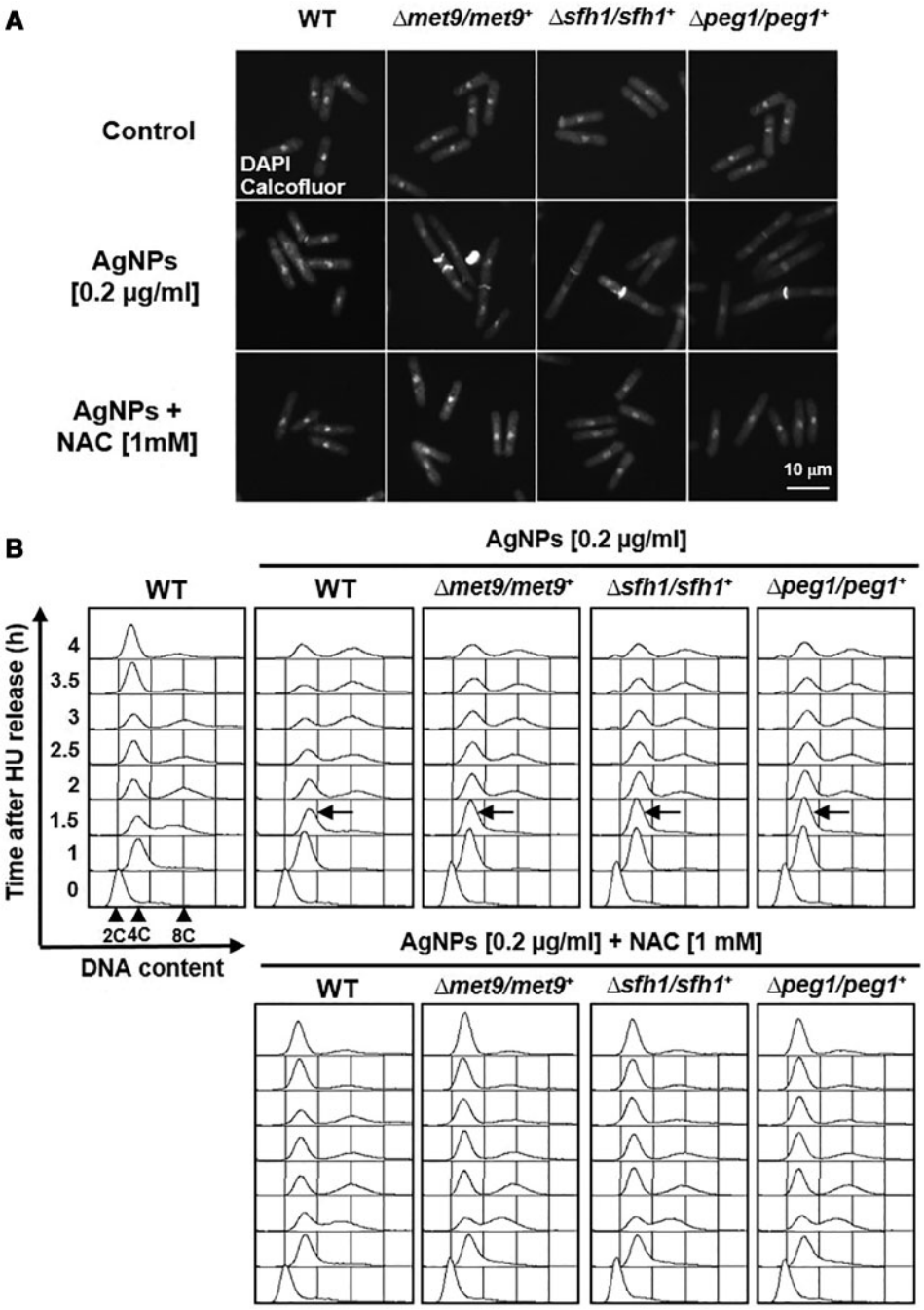


**Figure 4. AgNP-induced phenotypic changes and cell cycle arrest via reactive oxygen species (ROS) in the 3 essential AgNP targets**. A, Elongated phenotypic change induced by AgNPs in the 3 noble heterozygous AgNP targets (Δ*met9*/*met9*$^{+}$, Δ*sfh1*/*sfh1*$^{+}$, and Δ*peg1*/*peg1*$^{+}$). Cells were treated with 0.2 μg/ml AgNPs for 4 h, and their phenotypic changes in septa and nuclei were observed by fluorescence microscopy using DAPI and Calcofluor-white as staining dyes. Next, cells were pretreated with 1 mM N-acetylcysteine (NAC) prior to AgNP treatment and its effects on phenotype were observed. Their phenotypic changes were compared with those in the wild-type control cells. Magnification = 400×, Scale bar =10 μm. B, Cell cycle arrest by AgNPs in the 3 noble heterozygous AgNP targets (Δ*met9*/*met9*$^{+}$, Δ*sfh1*/*sfh1*$^{+}$, and Δ*peg1*/*peg1*$^{+}$). After synchronized cells were released from hydroxyurea, the cells were treated with 0.2 μg/ml AgNPs at the indicated time. The cell cycle patterns were analyzed by measuring the DNA contents (filled triangles) of cell populations using a flow cytometer. Notably, AgNPs increased the cell population with 4C DNA content (arrows) in the heterozygous AgNP targets compared with the wild-type control. Next, the cells were pretreated with 1 mM NAC prior to 0.2 μg/ml AgNPs and its effects on cell cycle were observed.

which was abrogated by NAC pretreatment (Figure 6D). Finally, the AgNP treatment of the *MTHFR* knockdown cells caused an extra cell cycle delay in the progression through sub-G1 phase (apoptotic cell populations) in addition to the S-phase delay in the mock control cells (Figure 6E). This effect was also abrogated by NAC pretreatment. Taken together, the AgNP treatment of the *MTHFR* knockdown cells caused oxidative DNA damage and subsequent cell cycle arrest in the sub-G1/S phases, leading to growth inhibition. Taken together, MTHFR plays a key role in cellular defense against ROS induced by AgNPs via NADPH production, implying that the functional role of MTHFR is well conserved from fission yeast to humans.

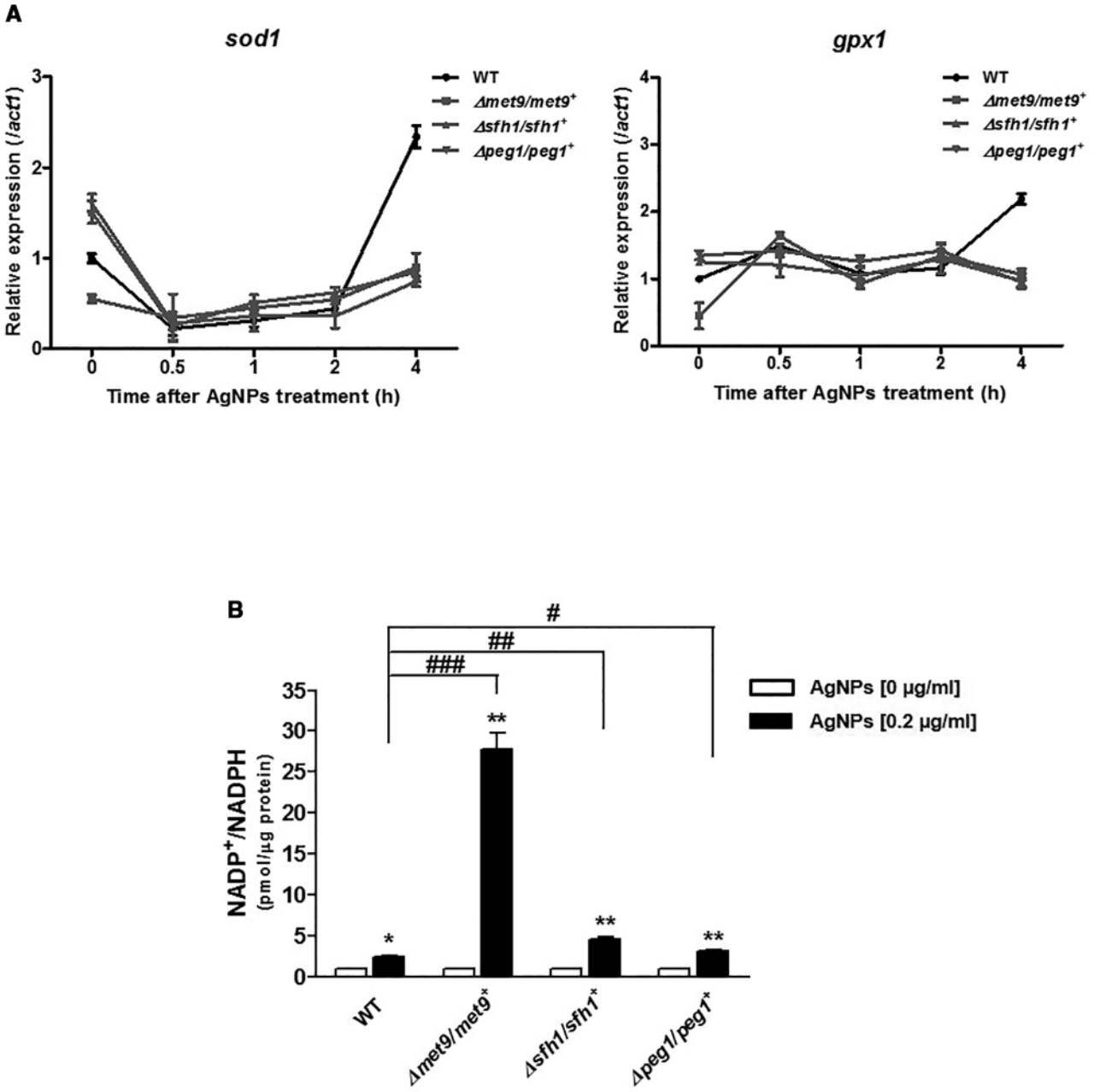


**Figure 5. AgNP-induced transcriptional changes in antioxidant enzymes and depletion of NADPH in the 3 essential AgNP targets.** A, Transcriptional pattern of antioxidant enzymes in the presence of AgNPs in the 3 noble heterozygous AgNP targets (Δ*met9*/*met9*$^+$, Δ*sfh1*/*sfh1*$^+$, and Δ*peg1*/*peg1*$^+$). Cells were treated with 0.2 μg/ml AgNPs for the indicated time, and their mRNA levels of *sod1* and *gpx1* were analyzed by q-PCR compared with the wild-type control ($n = 3$). B, AgNP-induced changes in NADP$^+$/NADPH contents in the 3 noble heterozygous AgNP targets (Δ*met9*/*met9*$^+$, Δ*sfh1*/*sfh1*$^+$, and Δ*peg1*/*peg1*$^+$). Cells were treated with 0.2 μg/ml AgNPs for 4 h, and the cellular level of NADP$^+$/NADPH was analyzed by the NADP$^+$/NADPH quantification colorimetric kit compared with the controls ($n = 3$, $*p < .05$ and $**p < .01$, treated vs untreated control cells; $\#p < .05$, $\#\#p < .01$, and $\#\#\#p < .001$, treated wild-type vs treated heterozygous deletion cells).

## DISCUSSION

To elucidate the mechanism of AgNP-induced cytotoxicity in a systematic way, so far, studies have been performed using many model organisms. Yeasts (Guo *et al.*, 2016; Okada *et al.*, 2014) also have been employed to screen target genes against a variety of stresses such as ROS, chemicals, or toxic metals. Recently, the gene deletion library of fission yeast was constructed by our group after budding yeast (Kim *et al.*, 2010), which opens a new era for the genome-wide screening of target genes against chemicals by the principle of drug-induced haploinsufficiency (Lum *et al.*, 2004). These studies normally use a haploid gene deletion library only consisting of nonessential genes for the systematic target screening against a stress inducer. In this study, to find AgNP targets on a genome-wide scale, we have applied, for the first time, a fission yeast heterozygous deletion library covering nearly all essential genes as well as nonessential genes. Thus, our trial using a heterozygous deletion library has the advantage of finding novel essential target genes. Although the genome-wide microarray screening system is convenient regarding time, this

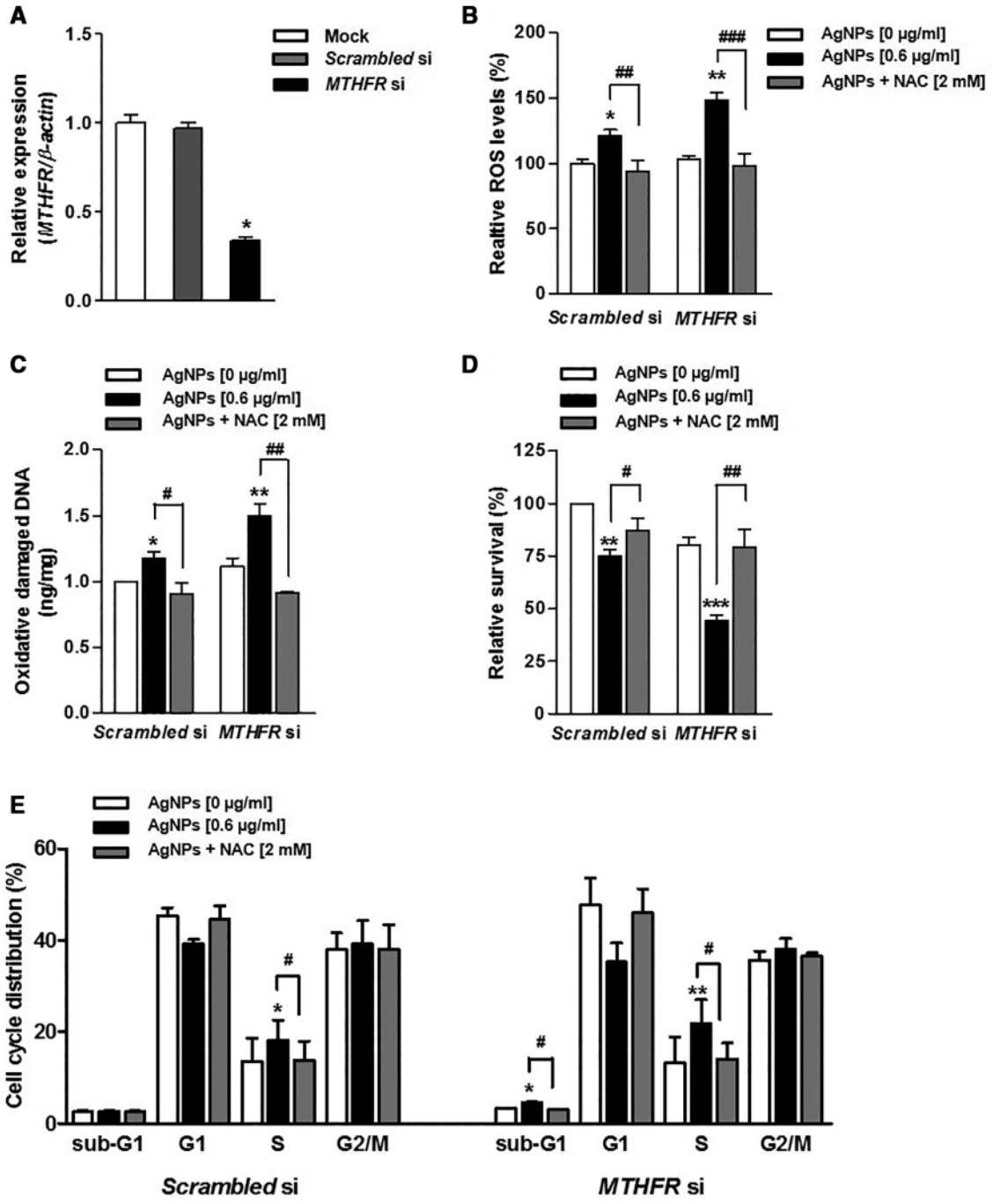


**Figure 6. Functional conservation of fission yeast *met*9 in human cell line HEK293.** A, Knockdown of *MTHFR* (*met*9 ortholog in human) in HEK293 by siRNA. Cells were transfected with scrambled or *MTHFR* si-RNA and their transcriptional levels were analyzed by quantitative PCR 72 h after the transfection. Relative expression levels were normalized to the mock transfection ($n = 3$, $*p < .05$). B, AgNP-induced reactive oxygen species (ROS) in si-*MTHFR* HEK293. After transfection with scrambled or *MTHFR* si-RNA, the cells were treated with or without 0.6 μg/ml AgNPs and their ROS levels were analyzed by FACS using $H_2$DCFDA as a fluorescent dye. Next, the cells were pretreated with 2 mM N-acetylcysteine (NAC) for 3 h prior to the AgNP treatment and their ROS levels were compared with ROS levels in unpretreated cells ($n = 3$, $*p < .05$ and $**p < .01$ AgNP-treated vs untreated cells; $\#\#p < .01$ and $\#\#\#p < .001$, NAC-treated vs untreated cells). C, AgNP-induced DNA damage via ROS in si-*MTHFR* HEK293. After transfection with scrambled or *MTHFR* si-RNA, the cells were treated with or without 0.6 μg/ml AgNPs and their 8-OHdG levels were measured as a DNA damage marker using OxiSelect Oxidative DNA damage ELISA kit. Next, the cells were pretreated with 2 mM NAC for 3 h prior to the AgNP treatment and their DNA damage was compared with DNA damage in unpretreated cells ($n = 3$, $*p < .05$ and $**p < .01$, AgNP-treated vs untreated cells; $\#p < .05$ and $\#\#p < .01$, NAC-treated vs untreated cells). D, AgNP-induced growth inhibition via ROS in si-*MTHFR* HEK293. After transfection with scrambled or *MTHFR* siRNA, the cells were treated with or without 0.6 μg/ml AgNPs and their survival rates were measured by an MTT assay. Next, the cells were pretreated with 2 mM NAC for 3 h prior to the AgNP treatment and their growth rate was compared with the growth rate of unpretreated cells ($n = 3$, $**p < .01$ and $***p < .001$, AgNP-treated vs untreated cells; $\#p < .05$ and $\#\#p < .01$, NAC-treated vs untreated cells). (E) AgNP-induced cell cycle arrest via ROS in si-*MTHFR* HEK293. After transfection with scrambled or *MTHFR* si-RNA, the cells were treated with or without 0.6 μg/ml AgNPs and their fraction at each cell cycle phase (sub-G1, G1, S, or G2/M) was measured by FACS. Next, the cells were pretreated with 2 mM NAC for 3 h prior to the AgNP treatment and their fraction at each cell cycle phase was compared with cell cycle patterns in unpretreated cells ($n = 3$, $*p < .05$ and $**p < .01$, AgNP-treated vs untreated cells; $\#p < .05$, NAC-treated vs untreated cells).

system needs to be validated by a one-by-one assay for confirmation. For example, the primary genome-wide screening has shown 11 false-positive targets, as judged by the spotting assay confirming the 33 targets (Table 1) out of the 44 primary genes screened. Furthermore, primary screening also missed many potential AgNP targets, including the 17 additional target genes associated with GO terms similar to those of the top 10 sensitive target genes, which were revealed by the cross-sensitivity hierarchical clustering analysis (Figure 2). However, the genome-wide screening system remains a useful tool for primary screening because the 35 randomly added genes (except 3 genes) were proven to be insensitive to AgNPs. One possible explanation is that the microarray analysis is not yet perfect due to an erroneous mismatch between the array chip and the bar code probe due to mutations. To improve the genome-wide screening method, we are in the progress of utilizing next-generation sequencing technology. This cutting-edge technology would better enable screenings by a direct counting of signals rather than the indirect hybridization of a microarray.

An accumulating body of evidence has shown that metal nanoparticles are absorbed into cells through a transport system called the "Trojan horse-type mechanism" (Limbach *et al.*, 2007). The intracellular AgNPs that interact with cellular components, such as proteins and thiols, become oxidized (Henglein, 1998; Lok *et al.*, 2007) and release $Ag^+$ (Liu and Hurt, 2010; Limbach *et al.*, 2007). In accordance with the previous reports, we also showed that AgNPs could penetrate yeast cells and release $Ag^+$, thereby resulting in cytotoxicity (Figure 1). Since all engineered nanoparticles have their own unique physical, chemical, and biological properties, they act as auxiliary factors for inducing cytotoxicity by themselves. However, AgNP-induced cytotoxicity is basically attributed to $Ag^+$ release via the generation of ROS, resulting in the depletion of redox potential levels, reduction of mitochondrial membrane potential, and subsequently damage of DNA and proteins (Kang *et al.*, 2012). Accordingly, AgNP targets should present a variety of genes related to reducing ROS levels. It was not surprising that the stress most similar to AgNPs was that induced by $Ag^+$, followed by that induced by the typical ROS inducer $H_2O_2$ (Figure 2). Like $H_2O_2$, metals such as As and Cd also have been previously described to induce ROS in systems from yeast strains to cell lines (Guo *et al.*, 2016; Kennedy *et al.*, 2008). In this regard, the 33 targets screened contain 9 genes related to antioxidant function, including 6 and 3 genes in the GO term of sulfur compound metabolism and signal transduction, respectively (Table 2). In the category of sulfur compound metabolism, our screening results revealed targets such as *gcs*1 and *gcs*2 related to the synthesis of GSH, which requires NADPH for the regeneration of its oxidized form GSSG (Birben *et al.*, 2012). In addition to the important reducing power molecule GSH (Pluskal *et al.*, 2016), the sulfide-quinone system is well known as an ROS defense system in a variety of organisms (Hildebrandt and Grieshaber, 2008) via the reduction of the antioxidant CoQ10 in the lipid fraction of the mitochondrial membrane (Bentinger *et al.*, 2007). The mitochondrial sulfide-quinone oxidoreductase, *hmt*2, has been screened, which we have previously reported as a defense enzyme against Cd in fission yeast (Kennedy *et al.*, 2008). Indeed, the human ortholog of *hmt2*, the *SQRDL* (sulfide-quinone oxidoreductase) gene, has been described to detoxify against hydrogen sulfide (Hourihan *et al.*, 2013). The other mitochondrial thiosulfate sulfurtransferase *rdl*2 also has been screened (Hildebrandt and Grieshaber, 2008; Melideo *et al.*, 2014). Since the deletion of *rdl*2 has been described to become sensitive to a sodium selenide exposure in budding yeast (Peyroche *et al.*, 2012), it would be related to AgNP-induced ROS. Also, phytochelatin synthase (*pcs*2) has been screened, which has been reported to be critical for Cd detoxification by producing the low-molecular-weight sulfur-containing peptide phytochelatin in plants (Cobbett, 2000). Oxidized phytochelatin gets reduced by the reducing power of GSH (Guo *et al.*, 2016). Another important GO term for the detoxification of AgNPs should be the signaling pathway to respond to oxidative stress. The *mcs*4 and *wis*4 genes screened have been previously reported to be key factors of the stress-activated protein kinase (SAPK) signaling cascade as an upstream regulator of Sty1 (also known as Spc1), which is important for the detoxification of oxidative stress (Rodriguez-Gabriel and Russell, 2005) and Cd (Kennedy *et al.*, 2008). For example, the PI3K and p38 MAPK signaling cascades have been described to engage in AgNP-induced cytotoxicity in human cells (Eom and Choi, 2010). However, microarray screening has missed the transcription factors in the p38 MAPK signaling cascade, including Pap1 and Atf1 (Table 1). They play a key role in concert for the transcriptional regulation of antioxidant genes such as *sod*1 and *gpx*1 against ROS-inducing stresses (Lee *et al.*, 2002; Yamada *et al.*, 1999), as shown in Figure 5. Intriguingly, we have found the SPCC1827.07c gene as an AgNP target, whose function is not yet clear in the signaling GO term. Since the SYG1 mutant in the budding yeast, the ortholog of fission yeast SPCC1827.07c has been reported to increase sulfur ($1^+$) accumulation with abnormal mitochondrial morphology against a variety of ion stresses (Yu *et al.*, 2012), such as excess manganese (Chesi *et al.*, 2012), the function of the unknown gene is likely to be related to a signaling pathway involved in ROS stresses.

Of particular interest are the 3 essential target genes related to the GO term of one-carbon metabolism by folate (*met*9) or cellular component organization (*peg*1 and *sfh*1). The *sfh*1 gene encoding the chromatin structure remodeling (RSC) complex subunit would be required for the effective transcription regulation of a series of defense genes against AgNPs (Uffenbeck and Krebs, 2006). The *peg*1 gene encoding the CLASP (cytoplasmic linker associated protein) family microtubule-associated protein would be critical for maintaining microtubule structure, as AgNPs have been reported to disrupt cytoskeleton components (Xu *et al.*, 2013). The *met*9 gene encoding MTHFR would be necessary for NADPH production, which supplies a variety of antioxidant enzymes with reducing power. Notably, the folate pathway has been suggested to be a pathway for producing cytosolic NADPH in addition to the canonical pentose-phosphate pathway (Fan *et al.*, 2014).

Next, we aimed to find the corresponding human orthologs of the 3 novel essential targets and determine their functional conservation in a human cell line. The *met*9 gene has been well conserved throughout evolution from bacteria to humans (Naula *et al.*, 2002; Yamada *et al.*, 2001), as all living organisms use NADPH as the basic reducing power molecule against ROS. Indeed, MTHFR has been described to be involved in many diseases when mutated (Frosst *et al.*, 1995; Ma *et al.*, 1996; van der Put *et al.*, 2001). For example, MTHFR deficiency causes a decreased level of folate, resulting in excess oxidative stress and increased plasma levels of homocysteine, called hyperhomocysteinemia (Ma *et al.*, 1996). A genetic variation in *MTHFR* (C677T) leads to vascular disease and neural tube defects via hyperhomocysteinemia (Frosst *et al.*, 1995; van der Put *et al.*, 2001) as well as mitochondrial dysfunction (Visalli *et al.*, 2015). Human orthologs for the essential genes *sfh1* and *peg1* could not

be found. Likely, the cellular component organization is different between lower single-cell yeasts and higher multicellular organisms.

As far as we know, this is the first study claiming that the *met*9 essential gene is critical for the cellular defense of the AgNP-mediated toxicity in fission yeast via the regulation of NADPH and that its relevance is conserved in a human cell line. Also, the results support the recent discovery as a proof of concept saying that the folate cycle plays a key role for NADPH production along with the canonical oxidative pentose pathway (Fan *et al.*, 2014). Since MTHFR may be a possible drug target for ROS-related diseases, further study is necessary for elucidation of the mechanism by which MTHFR plays a key role against ROS in human cells.

## SUPPLEMENTARY DATA

Supplementary data are available at *Toxicological Sciences* online.

## FUNDING

National Research Foundation (NRF) grants funded by the Korean Government, Ministry of Science and ICT (NRF-2012M3A9D1054667 and NRF-2017M3A9B5060880); National Research Council of Science and Technology (grant no. DRC-15-01-KRICT); Chungnam National University.

## AUTHORS' CONTRIBUTIONS

D.U.K. and K.L.H. conceived the project; A.R.L., S.J.L., M.L., M.N., S.L., J.C., and H.J.L. performed experiments and data analysis; M.L. performed bioinformatics; A.R.L., S.J.L., D.U.K., and K.L.H. wrote the paper.

## ACKNOWLEDGMENTS

D.U.K. and S.J.L. were supported by KRIBB and Chonbuk National University, respectively. The remaining authors have no conflicts of interest to declare.

## REFERENCES

Asharani, P., Sethu, S., Lim, H. K., Balaji, G., Valiyaveettil, S., and Hande, M. P. (2012). Differential regulation of intracellular factors mediating cell cycle, DNA repair and inflammation following exposure to silver nanoparticles in human cells. *Genome Integr.* **3**, 2.

AshaRani, P. V., Low Kah Mun, G., Hande, M. P., and Valiyaveettil, S. (2009). Cytotoxicity and genotoxicity of silver nanoparticles in human cells. *ACS Nano.* **3**, 279–290.

Bell, R. A., and Kramer, J. R. (1999). Structural chemistry and geochemistry of silver–sulfur compounds: Critical review. *Environ. Toxicol. Chem.* **18**, 9–22.

Bentinger, M., Brismar, K., and Dallner, G. (2007). The antioxidant role of coenzyme Q. *Mitochondrion* **7(Suppl)**, S41–S50.

Birben, E., Sahiner, U. M., Sackesen, C., Erzurum, S., and Kalayci, O. (2012). Oxidative stress and antioxidant defense. *World Allergy Organ. J.* **5**, 9–19.

Cadet, J., Douki, T., Gasparutto, D., and Ravanat, J. L. (2003). Oxidative damage to DNA: Formation, measurement and biochemical features. *Mutat. Res.* **531**, 5–23.

Carlson, C., Hussain, S. M., Schrand, A. M., Braydich-Stolle, L. K., Hess, K. L., Jones, R. L., and Schlager, J. J. (2008). Unique cellular interaction of silver nanoparticles: Size-dependent generation of reactive oxygen species. *J. Phys. Chem. B* **112**, 13608–13619.

Chen, X., and Schluesener, H. J. (2008). Nanosilver: A nanoproduct in medical application. *Toxicol. Lett.* **176**, 1–12.

Chesi, A., Kilaru, A., Fang, X., Cooper, A. A., Gitler, A. D., and Kahle, P. J. (2012). The role of the Parkinson's disease gene PARK9 in essential cellular pathways and the manganese homeostasis network in yeast. *PLoS One* **7**, e34178.

Chung, W. H., Kim, K. D., Cho, Y. J., and Roe, J. H. (2004). Differential expression and role of two dithiol glutaredoxins Grx1 and Grx2 in *Schizosaccharomyces pombe*. *Biochem. Biophys. Res. Commun.* **321**, 922–929.

Cobbett, C. S. (2000). Phytochelatins and their roles in heavy metal detoxification. *Plant Physiol.* **123**, 825–832.

Damm, C., and Münstedt, H. (2008). Kinetic aspects of the silver ion release from antimicrobial polyamide/silver nanocomposites. *Appl. Phys. A: Mater. Sci. Process* **91**, 479–486.

Drake, P. L., and Hazelwood, K. J. (2005). Exposure-related health effects of silver and silver compounds: A review. *Ann. Occup. Hyg.* **49**, 575–585.

Eom, H. J., and Choi, J. (2010). p38 MAPK activation, DNA damage, cell cycle arrest and apoptosis as mechanisms of toxicity of silver nanoparticles in Jurkat T cells. *Environ. Sci. Technol.* **44**, 8337–8342.

Fan, J., Ye, J., Kamphorst, J. J., Shlomi, T., Thompson, C. B., and Rabinowitz, J. D. (2014). Quantitative flux analysis reveals folate-dependent NADPH production. *Nature* **510**, 298–302.

Farrugia, G., and Balzan, R. (2012). Oxidative stress and programmed cell death in yeast. *Front. Oncol.* **2**, 64.

Fodinger, M., Horl, W. H., and Sunder-Plassmann, G. (2000). Molecular biology of 5, 10-methylenetetrahydrofolate reductase. *J. Nephrol.* **13**, 20–33.

Frosst, P., Blom, H. J., Milos, R., Goyette, P., Sheppard, C. A., Matthews, R. G., Boers, G. J. H., den Heijer, M., Kluijtmans, L. A. J., van den Heuve, L. P., *et al.* (1995). A candidate genetic risk factor for vascular disease: a common mutation in methylenetetrahydrofolate reductase. *Nat. Genet.* **10**, 111–113.

Grant, C. M. (2001). Role of the glutathione/glutaredoxin and thioredoxin systems in yeast growth and response to stress conditions. *Mol. Microbiol.* **39**, 533–541.

Gliga, A. R., Skoglund, S., Wallinder, I. O., Fadeel, B., and Karlsson, H. L. (2014). Size-dependent cytotoxicity of silver nanoparticles in human lung cells: the role of cellular uptake, agglomeration and Ag release. *Part. Fibre Toxicol.* **11**, 11–17.

Guo, L., Ganguly, A., Sun, L., Suo, F., Du, L. L., and Russell, P. (2016). Global fitness profiling identifies arsenic and cadmium tolerance mechanisms in fission yeast. *G3 (Bethesda)* **6**, 3317–3333.

Halliwell, B., and Aruoma, O. I. (1991). DNA damage by oxygen-derived species. Its mechanism and measurement in mammalian systems. *FEBS Lett.* **281**, 9–19.

Han, S., Lee, M., Chang, H., Nam, M., Park, H. O., Kwak, Y. S., Ha, H. J., Kim, D., Hwang, S. O., Hoe, K. L., *et al.* (2013). Construction of the first compendium of chemical-genetic profiles in the fission yeast *Schizosaccharomyces pombe* and comparative compendium approach. *Biochem. Biophys. Res. Commun.* **436**, 613–618.

Henglein, A. (1998). Colloidal silver nanoparticles: Photochemical preparation and interaction with $O_2$, $CCl_4$, and some metal. *Chem. Mater.* **10**, 444–450.

Hildebrandt, T. M., and Grieshaber, M. K. (2008). Three enzymatic activities catalyze the oxidation of sulfide to thiosulfate in mammalian and invertebrate mitochondria. *FEBS J.* **275**, 3352–3361.

Hourihan, J. M., Kenna, J. G., and Hayes, J. D. (2013). The gasotransmitter hydrogen sulfide induces Nrf2-target genes by inactivating the Keap1 ubiquitin ligase substrate adaptor through formation of a disulfide bond between Cys-226 and Cys-613. *Antioxid. Redox Signal* **19**, 465–481.

Jakobsson-Borin, A., Aberg, F., and Dallner, G. (1994). Lipid peroxidation of microsomal and mitochondrial membranes extracted with n-pentane and reconstituted with ubiquinol, dolichol and cholesterol. *Biochim. Biophys. Acta* **1213**, 159–166.

Jung, W. K., Koo, H. C., Kim, K. W., Shin, S., Kim, S. H., and Park, Y. H. (2008). Antibacterial activity and mechanism of action of the silver ion in *Staphylococcus aureus* and *Escherichia coli*. *Appl. Environ. Microbiol.* **74**, 2171–2178.

Kang, S. J., Lee, Y. J., Lee, E. K., and Kwak, M. K. (2012). Silver nanoparticles-mediated G2/M cycle arrest of renal epithelial cells is associated with NRF2-GSH signaling. *Toxicol. Lett.* **211**, 334–341.

Kennedy, P. J., Vashisht, A. A., Hoe, K. L., Kim, D. U., Park, H. O., Hayles, J., and Russell, P. (2008). A genome-wide screen of genes involved in cadmium tolerance in *Schizosaccharomyces pombe*. *Toxicol. Sci.* **106**, 124–139.

Kim, D. U., Hayles, J., Kim, D., Wood, V., Park, H. O., Won, M., Yoo, H. S., Duhig, T., Nam, M., Palmer, G., *et al.* (2010). Analysis of a genome-wide set of gene deletions in the fission yeast *Schizosaccharomyces pombe*. *Nat. Biotechnol.* **28**, 617–623.

Lee, J., Kwon, E. S., Kim, D. W., Cha, J., and Roe, J. H. (2002). Regulation and the role of Cu, Zn-containing superoxide dismutase in cell cycle progression of *Schizosaccharomyces pombe*. *Biochem. Biophys. Res. Commun.* **297**, 854–862.

Limbach, L. K., Wick, P., Manser, P., Grass, R. N., Bruinink, A., and Stark, W. J. (2007). Exposure of engineered nanoparticles to human lung epithelial cells: Influence of chemical composition and catalytic activity on oxidative stress. *Environ. Sci. Technol.* **41**, 4158–4163.

Liu, J., and Hurt, R. H. (2010). Ion release kinetics and particle persistence in aqueous nano-silver colloids. *Environ. Sci. Technol.* **44**, 2169–2175.

Lok, C. N., Ho, C. M., Chen, R., He, Q. Y., Yu, W. Y., Sun, H., Tam, P. K., Chiu, J. F., and Che, C. M. (2007). Silver nanoparticles: Partial oxidation and antibacterial activities. *J. Biol. Inorg. Chem.* **12**, 527–534.

Lum, P. Y., Armour, C. D., Stepaniants, S. B., Cavet, G., Wolf, M. K., Butler, J. S., Hinshaw, J. C., Garnier, P., Prestwich, G. D., Leonardson, A., *et al.* (2004). Discovering modes of action for therapeutic compounds using a genome-wide screen of yeast heterozygotes. *Cell* **116**, 121–137.

Ma, J., Stampfer, M. J., Hennekens, C. H., Frosst, P., Selhub, J., Horsford, J., Malinow, M. R., Willett, W. C., and Rozen, R. (1996). Methylenetetrahydrofolate reductase polymorphism, plasma folate, homocysteine, and risk of myocardial infarction in US physicians. *Circulation* **94**, 2410–2416.

Melideo, S. L., Jackson, M. R., and Jorns, M. S. (2014). Biosynthesis of a central intermediate in hydrogen sulfide metabolism by a novel human sulfurtransferase and its yeast ortholog. *Biochemistry* **53**, 4739–4753.

Moreno, S., Klar, A., and Nurse, P. (1991). Molecular genetic analysis of fission yeast *Schizosaccharomyces pombe*. *Methods Enzymol.* **194**, 795–823.

Nair, P. M., and Chung, I. M. (2014). Assessment of silver nanoparticle-induced physiological and molecular changes in *Arabidopsis thaliana*. *Environ. Sci. Pollut. Res Int.* **21**, 8858–8869.

Naula, N., Walther, C., Baumann, D., and Schweingruber, M. E. (2002). Two non-complementing genes encoding enzymatically active methylenetetrahydrofolate reductases control methionine requirement in fission yeast *Schizosaccharomyces pombe*. *Yeast* **19**, 841–848.

Navarro, E., Piccapietra, F., Wagner, B., Marconi, F., Kaegi, R., Odzak, N., Sigg, L., and Behra, R. (2008). Toxicity of silver nanoparticles to *Chlamydomonas reinhardtii*. *Environ. Sci. Technol.* **42**, 8959–8964.

Nurse, P. (1994). Fission yeast morphogenesis–posing the problems. *Mol. Biol. Cell* **5**, 613–616.

Okada, N., Ogawa, J., and Shima, J. (2014). Comprehensive analysis of genes involved in the oxidative stress tolerance using yeast heterozygous deletion collection. *FEMS Yeast Res.* **14**, 425–434.

Perrone, G. G., Tan, S. X., and Dawes, I. W. (2008). Reactive oxygen species and yeast apoptosis. *Biochim. Biophys. Acta* **1783**, 1354–1368.

Peyroche, G., Saveanu, C., Dauplais, M., Lazard, M., Beuneu, F., Decourty, L., Malabat, C., Jacquier, A., Blanquet, S., Plateau, P., and Rishi, A. (2012). Sodium selenide toxicity is mediated by O2-dependent DNA breaks. *PLoS One* **7**, e36343.

Pluskal, T., Sajiki, K., Becker, J., Takeda, K., and Yanagida, M. (2016). Diverse fission yeast genes required for responding to oxidative and metal stress: Comparative analysis of glutathione-related and other defense gene deletions. *Genes Cells* **21**, 530–542.

Rodriguez-Gabriel, M. A., and Russell, P. (2005). Distinct signaling pathways respond to arsenite and reactive oxygen species in *Schizosaccharomyces pombe*. *Eukaryot. Cell* **4**, 1396–1402.

Roh, J. Y., Sim, S. J., Yi, J., Park, K., Chung, K. H., Ryu, D. Y., and Choi, J. (2009). Ecotoxicity of silver nanoparticles on the soil nematode *Caenorhabditis elegans* using functional ecotoxicogenomics. *Environ. Sci. Technol.* **43**, 3933–3940.

Stadtman, E. R. (1993). Oxidation of free amino acids and amino acid residues in proteins by radiolysis and by metal-catalyzed react. *Annu. Rev. Biochem.* **62**, 797–821.

Uffenbeck, S. R., and Krebs, J. E. (2006). The role of chromatin structure in regulating stress-induced transcription in *Saccharomyces cerevisiae*. *Biochem. Cell Biol.* **84**, 477–489.

Valko, M., Morris, H., and Cronin, M. T. (2005). Metals, toxicity and oxidative stress. *Curr. Med. Chem.* **12**, 1161–1208.

van der Put, N. M., van Straaten, H. W., Trijbels, F. J., and Blom, H. J. (2001). Folate, homocysteine and neural tube defects: An overview. *Exp. Biol. Med. (Maywood)* **226**, 243–270.

Visalli, G., Bertuccio, M. P., Picerno, I., Spataro, P., and Di Pietro, A. (2015). Mitochondrial dysfunction by pro-oxidant vanadium: Ex vivo assessment of individual susceptibility. *Environ. Toxicol. Pharmacol.* **39**, 93–101.

Xu, F., Piett, C., Farkas, S., Qazzaz, M., and Syed, N. I. (2013). Silver nanoparticles (AgNPs) cause degeneration of cytoskeleton and disrupt synaptic machinery of cultured cortical neurons. *Mol. Brain* **6**, 29.

Yamada, K., Chen, Z., Rozen, R., and Matthews, R. G. (2001). Effects of common polymorphisms on the properties of recombinant human methylenetetrahydrofolate reductase. *Proc. Natl. Acad. Sci. U.S.A.* **98**, 14853–14858.

Yamada, K., Nakagawa, C. W., and Mutoh, N. (1999). *Schizosaccharomyces pombe* homologue of glutathione peroxidase, which does not contain selenocysteine, is induced by several stresses and works as an antioxidant. *Yeast* **15**, 1125–1132.

Yamanaka, M., Hara, K., and Kudo, J. (2005). Bactericidal act of a silver ion solution on *Escherichia coli*, studied by energy-filtering transmission electron microscopy and proteomic analysis. *Appl. Environ. Microbiol.* **71**, 7589–7593.

Yu, D., Danku, J. M., Baxter, I., Kim, S., Vatamaniuk, O. K., Vitek, O., Ouzzani, M., and Salt, D. E. (2012). High-resolution genome-wide scan of genes, gene-networks and cellular systems impacting the yeast ionome. *BMC Genom.* **13**, 623.

Zhang, F., Lau, S. S., and Monks, T. J. (2011). The cytoprotective effect of N-acetyl-L-cysteine against ROS-induced cytotoxicity is independent of its ability to enhance glutathione synthesis. *Toxicol. Sci.* **120**, 87–97.